

1 **LMO2 is critical for early metastatic events in breast cancer**

2 **Authors:**

3 Shaheen Sikandar<sup>1,†,\*</sup>, Jane Antony<sup>1,†</sup>, Gunsagar S. Gulati<sup>1,†</sup>, Angera H. Kuo<sup>1</sup>, William  
4 Hai Dang Ho<sup>1</sup>, Soumyashree Das<sup>2</sup>, Chloé B. Steen<sup>3</sup>, Thiago Almeida Pereira<sup>1</sup>, Dalong  
5 Qian<sup>1</sup>, Philip A. Beachy<sup>1</sup>, Fredrick Dirbas<sup>4</sup>, Kristy Red-Horse<sup>1,2</sup>, Terence H. Rabbitts<sup>5</sup>,  
6 Jean Paul Thiery<sup>6</sup>, Aaron M. Newman<sup>1,7,‡</sup>, and Michael F. Clarke<sup>1,8,‡,\*</sup>

7 **Affiliations:**

8 <sup>1</sup>Institute for Stem Cell Biology and Regenerative Medicine, 265 Campus Drive, School of Medicine,  
9 Stanford, CA-94305.

10 <sup>2</sup>Department of Biology, Stanford University, Stanford, CA 94305, USA.

11 <sup>3</sup>Division of Oncology, Department of Medicine, Stanford Cancer Institute, Stanford University, Stanford,  
12 CA, USA.

13 <sup>4</sup>Department of Surgery, Stanford University School of Medicine, Stanford Cancer Institute, 875 Blake  
14 Wilbur Drive, Rm CC2235, Stanford, CA, 94305, USA.

15 <sup>5</sup>Institute of Cancer Research, Division of Cancer Therapeutics, London, SM2 5NG, UK.

16 <sup>6</sup>Bioland Laboratory, Guangzhou Regenerative Medicine and Health, Guangzhou, China.

17 <sup>7</sup>Department of Biomedical Data Science, Stanford University, Stanford, CA 94305, USA.

18 <sup>8</sup>Department of Medicine, Stanford University, Stanford, CA 94305, USA.

19 <sup>†</sup>These authors contributed equally.

20 <sup>‡</sup>Co-senior authors

21 \*Correspondence to: [mfclarke@stanford.edu](mailto:mfclarke@stanford.edu), [ssikanda@ucsc.edu](mailto:ssikanda@ucsc.edu)

22 **One sentence summary:**

23 LMO2 modulates STAT3 signaling in breast cancer metastasis.

## 24 **SUMMARY**

25 Metastasis is responsible for the majority of breast cancer-related deaths, however  
26 identifying the cellular determinants of metastasis has remained challenging. Here, we  
27 identified a minority population of immature *THY1<sup>+</sup>/VEGFA<sup>+</sup>* tumor epithelial cells in  
28 human breast tumor biopsies that display angiogenic features and are marked by the  
29 expression of the oncogene, *LMO2*. Higher abundance of *LMO2<sup>+</sup>* basal cells correlated  
30 with tumor endothelial content and predicted poor distant recurrence-free survival in  
31 patients. Using *MMTV-PyMT/Lmo2<sup>CreERT2</sup>* mice, we demonstrated that *Lmo2* lineage-  
32 traced cells have a higher propensity to metastasize. *LMO2* knockdown in human  
33 breast tumors reduced lung metastasis by impairing intravasation, leading to a reduced  
34 frequency of circulating tumor cells. Mechanistically, we find that *LMO2* binds to *STAT3*  
35 and is required for *STAT3* activation by *TNF $\alpha$*  and *IL6*. Collectively, our study identifies  
36 a population of metastasis-initiating cells with angiogenic features and establishes the  
37 *LMO2-STAT3* signaling axis as a therapeutic target in breast cancer metastasis.

## 38 **INTRODUCTION**

39 While significant progress has been made to treat early-stage breast cancer, treatment  
40 options and outcomes for metastatic breast cancer have been largely unchanged in a  
41 decade (Esposito et al., 2021; Siegel et al., 2011; Siegel et al., 2021). In order to  
42 improve outcomes for breast cancer patients, it is critical to identify and elucidate  
43 signaling pathways active in metastatic cells. However, it has been difficult to pinpoint  
44 cancer cell populations involved in metastasis as they represent a transient state (Lu  
45 and Kang, 2019). Previous studies employing lineage tracing and cell surface marker  
46 profiling have implicated distinct subsets of tumor epithelial cells in breast cancer  
47 metastasis, primarily using lineage markers such as E-cadherin (Beerling et al., 2016,  
48 Padmanaban et al., 2019), N-cadherin (Li et al., 2020) and S100a4 (Fischer et al.,  
49 2015). Recent studies have also suggested that metastatic cells display hybrid features  
50 of both epithelial and mesenchymal lineages (Kröger et al., 2019; Pastushenko et al.,

51 2021). This has led to a debate in the field about the precise molecular identity of  
52 metastasis-initiating cells (Lu and Kang, 2019; Shen and Kang, 2019; Ye et al., 2017).

53 Our previous work has demonstrated that in breast cancer, minority populations of  
54 phenotypically immature cells in the tumor are enriched in tumor-initiating potential and  
55 metastasis (Al-Hajj et al., 2003; Liu et al., 2010; Sikandar et al., 2017). Recent  
56 advances in single-cell technologies have revealed complex transcriptional landscapes  
57 in human tumors and enabled precise molecular characterization of these minority cell  
58 populations (Lawson et al., 2018). However, the functional and clinical significance of  
59 these populations remains to be elucidated (Lawson et al., 2018; Tanay and Regev,  
60 2017). To understand the transcriptional heterogeneity in breast cancer, we performed  
61 single-cell RNA sequencing (scRNA-seq) in primary patient samples and developed a  
62 novel computational method that can predict immature cell populations *in silico* (Gulati  
63 et al., 2020). Using our scRNA-seq data, bulk tumor expression deconvolution, lineage  
64 tracing, and functional assays, we have now identified a clinically relevant population of  
65 metastasis-initiating cells that express the hematopoietic transcription factor and T-cell  
66 oncogene, LMO2. Here, we mechanistically define the role of LMO2 in breast cancer  
67 metastasis by its association with tumor vasculature and identify LMO2 as a previously  
68 unknown regulator of STAT3 signaling in breast cancer.

## 69 RESULTS

### 70 **LMO2 is expressed in a minority population of immature THY1<sup>+</sup>/VEGFA<sup>+</sup> human 71 breast cancer cells.**

72 To understand the substructure of the epithelial populations in breast cancer, we started  
73 by analyzing scRNA-seq profiles (Gulati et al., 2020) of human breast tumor epithelial  
74 cells from patients with triple-negative ( $n = 5$ ) or estrogen receptor positive (ER<sup>+</sup>) breast  
75 cancer ( $n = 13$ ). We identified a minority population of THY1<sup>+</sup> cells that were largely  
76 restricted to the basal compartment, comprising 11% of all basal cells (**Fig. S1A, Table  
77 S1**). Moreover, within this subset, 33% of cells expressed VEGFA (**Fig. S1A**). We were  
78 struck by this combination since THY1<sup>+</sup> cells are enriched in reconstitution potential in

79 the normal mammary gland (Lobo et al., 2018) and tumorigenic potential in mouse  
80 tumors (Cho et al., 2008) and VEGFA is a pro-angiogenic factor linked to tumor growth  
81 and distant metastasis (Mercurio et al., 2005; Zhao et al., 2015). To determine whether  
82 *THY1*<sup>+</sup>/*VEGFA*<sup>+</sup> cells represent a potential immature cell population, we applied  
83 CytoTRACE, a computational framework for predicting cellular differentiation status on  
84 the basis of single-cell transcriptional diversity (Gulati et al., 2020). We found that  
85 relative to other basal cells, *THY1*<sup>+</sup>/*VEGFA*<sup>+</sup> cells are predicted to be significantly less  
86 differentiated, suggesting a role for this population in tumor growth or metastasis (**Fig.**  
87 **1A**).

88 To identify potential molecular regulators within this population, we next searched for  
89 genes with expression patterns that overlap *THY1* and *VEGFA* expression in our  
90 dataset. Intriguingly, we found that *LMO2*, a hematopoietic stem cell regulator (Yamada  
91 et al., 1998) and T-cell oncogene (Larson, 1995), was among the top five hits (**Fig. 1B**,  
92 **Table S2**). *LMO2* also marked *THY1*<sup>+</sup>/*VEGFA*<sup>+</sup> cells in an independent scRNA-seq atlas  
93 of triple-negative human breast tumors (Kim et al., 2018), corroborating this result (**Fig.**  
94 **1C**). Analysis of the *LMO2*<sup>+</sup> basal epithelial subset showed that these cells not only  
95 express *THY1* and epithelial cytokeratins (**Fig. 1D**), but also display a coherent gene  
96 expression program significantly enriched in angiogenesis genes, including *VEGFA* and  
97 *S100A4* (**Fig. 1E, Table S3**).

98 We next measured the relative abundance of distinct endothelial, immune, stromal, and  
99 epithelial populations in human breast tumors with respect to *LMO2*<sup>+</sup> basal cells. As  
100 *LMO2* is expressed in myriad cell types, including immune, stromal, and endothelial  
101 cells, the expression of the gene is insufficient to distinguish cell types. Therefore, we  
102 defined unique transcriptional signatures for various niche and breast epithelial cells  
103 from our scRNA-seq data and utilized CIBERSORTx, a deconvolution approach, to  
104 calculate the cellular composition of bulk RNA admixtures from breast cancer clinical  
105 cohorts (Newman et al., 2019) (**Methods**). In line with our previous results, we  
106 observed a striking correlation between the abundance of *LMO2*<sup>+</sup> basal cells and

107 endothelial cell content imputed in 508 breast tumors (Esserman et al., 2012) ( $r = 0.45$ ;  
108  $P < 2 \times 10^{-16}$ ; **Fig. 1F**).

109 **Human *LMO2*<sup>+</sup> basal cells are associated with poor outcomes in breast cancer**  
110 **patients.**

111 Deconvolution of an additional 3,024 human breast tumors from three clinical cohorts  
112 (Curtis et al., 2012; TCGA, 2012) revealed that basal *LMO2*<sup>+</sup> cells are more abundant in  
113 'Basal' breast cancer subtypes which correlate with more aggressive breast cancers as  
114 compared to other PAM50 classes (Perou et al., 2000) (**Fig. S1B**). We also found a  
115 significant increase in basal *LMO2*<sup>+</sup> cells with worsening clinical grade and stage of the  
116 tumor (**Fig. S1C, D**), suggesting that *LMO2*<sup>+</sup> cells increase with tumor progression.  
117 Importantly, higher levels of *LMO2*<sup>+</sup> basal cells were significantly associated with inferior  
118 distant recurrence-free survival (**Fig. 1G**), independent of estrogen receptor status.  
119 These data link the abundance of *LMO2*<sup>+</sup> basal epithelial cells with more aggressive  
120 breast tumors and distant metastasis.

121 ***Lmo2* lineage-traced cells have a higher propensity to metastasize.**

122 To experimentally verify our *in silico* findings, we began by employing the CreERT2  
123 system (Rios et al., 2014; van Amerongen et al., 2012; Van Keymeulen et al., 2011) to  
124 delineate the fate of epithelial cells that have expressed *LMO2*<sup>+</sup> in breast tumors. We  
125 obtained *Lmo2*<sup>CreERT2</sup> mice (Forster, Drynan, Pannell, Rabbits *in preparation*) and  
126 crossed them to *Rosa26*<sup>mTmG</sup> reporter and *MMTV-PyMT* tumor mice to generate triple-  
127 transgenic *Lmo2*<sup>CreERT2</sup>/*Rosa26*<sup>mTmG</sup>/*MMTV-PyMT* mice, which we termed *Lmo2-PyMT*  
128 (**Fig. 2A**). *MMTV-PyMT* tumors are an aggressive luminal subtype of breast cancer  
129 (Herschkowitz et al., 2007) that metastasize to the lungs (Guy et al., 1992) and have  
130 been extensively used to explore the cellular underpinnings of breast cancer metastasis  
131 (Beerling et al., 2016; Fischer et al., 2015; Padmanaban et al., 2019; Pastushenko et  
132 al., 2018). As *Lmo2* is expressed in other cells such as stromal and endothelial cells  
133 (Gratzinger et al., 2009), we orthotopically transplanted lineage depleted (CD45<sup>-</sup>/CD31<sup>-</sup>  
134 /Ter119<sup>-</sup>) tumor cells from TdTomato-fluorescent *Lmo2-PyMT* into non-fluorescent BL6  
135 mice to clearly assess the contribution of *Lmo2* lineage-traced breast cancer cells from

136 the tumor. After tumors were formed, we pulsed the mice with tamoxifen to induce  
137 expression of GFP in *Lmo2*-expressing cells (**Fig. 2B**). At 48h post-pulse, we verified  
138 that expression of *Lmo2* was enriched in the transplanted GFP<sup>+</sup> cancer cells (**Figs. 2C**,  
139 **S2**, and **S3A**). FACS quantification demonstrated that GFP<sup>+</sup> cells represented a minor  
140 fraction of all tumor cells and expressed the epithelial marker, EpCAM (**Fig. 2C**).

141 To assess the population dynamics of *Lmo2* lineage-traced cells, we plated TdTomato<sup>+</sup>  
142 tumor cells from *Lmo2-PyMT* mice in 3D organoid assays and pulsed the organoids with  
143 4-hydroxytamoxifen. Consistent with the *in vivo* model, lineage-traced GFP<sup>+</sup> cells  
144 comprised a minority of tumor organoids (~2%) 7 days post-pulse. This percentage was  
145 unchanged even after 4 weeks in culture, suggesting similar proliferative capacity  
146 between GFP<sup>+</sup> and TdTomato<sup>+</sup> cells (**Fig. S3B**). We confirmed this by plating sorted  
147 GFP<sup>+</sup> and TdTomato<sup>+</sup> cells in 3D organoid cultures and showing that both populations  
148 formed organoids at similar frequencies (**Fig. S3C**).

149 To determine whether *Lmo2*<sup>+</sup> cells co-associate with endothelial cells, as predicted *in*  
150 *silico* (**Fig. 1F**), we stained vasculature with endomucin and visualized their co-  
151 localization with 3D imaging. We found that *Lmo2* lineage-traced cells not only resided  
152 near tumor blood vessels (**Fig. 2E**) but surprisingly ~20% showed co-localization with  
153 tumor vasculature and appeared to be incorporated into the tumor vasculature (**Fig. 2E**  
154 and **S3D**).

155 Given that abundance of *LMO2*<sup>+</sup> cells in patients predicts distant recurrence-free  
156 survival (**Fig. 1G**) and *Lmo2* lineage-traced cells reside closer to tumor vasculature, we  
157 next tested whether *Lmo2*<sup>+</sup> cells have metastatic capabilities. As dissemination of  
158 metastatic cells occurs continuously during tumor growth, to lineage-trace tumor cells  
159 expressing *Lmo2*, we pulsed *Lmo2-PyMT* mice with tamoxifen 2-3 times per week once  
160 the tumors were palpable and continued until tumor endpoint (**see Methods; Fig. 3F**).  
161 At the end of the experiment, we found that in the primary tumor only 10-15% of tumor  
162 cells were GFP<sup>+</sup> (**Fig. 2G**). Surprisingly, even though the tumor was majority  
163 TdTomato<sup>+</sup>, the lungs had a disproportionately higher number of GFP<sup>+</sup> metastases,

164 several of which were also larger than the TdTomato<sup>+</sup> metastases ( $P = 0.034$ , Wilcoxon  
165 signed-rank unpaired test) (**Fig. 2H**). These data suggest that *Lmo2* lineage-traced cells  
166 have a higher propensity to form metastases in the *PyMT* mice and is consistent with  
167 our findings in human breast cancer patients (**Fig. 1G**). Furthermore, a subset of GFP  
168 tumor cells did not remain *Lmo2* positive (**Fig. S3E**), suggesting that expression of  
169 *Lmo2* in some cells represents a transient state, in agreement with previous studies  
170 linking transient cell states to metastases (Pastushenko et al., 2018).

171 ***LMO2* knockdown abrogates lung metastasis in human breast cancer models.**

172 To understand the functional role of *LMO2* in human breast cancer, we knocked down  
173 *LMO2* expression in MDA-MB-468 cells using two independent shRNA vectors tagged  
174 with a GFP reporter (**Fig. S4A-C**). We then implanted the cells orthotopically in  
175 immunodeficient mice (**Fig. 3A** and **S4D**). In contrast to a previous report (Liu et al.,  
176 2016), knockdown of *LMO2* did not affect primary tumor growth (**Fig. 3B**) or proliferation  
177 *in vitro* (**Fig. S5A**). Nevertheless, *LMO2*-knockdown tumors had significantly fewer lung  
178 metastases relative to control ( $P = 0.003$ , ANOVA; **Fig. 2C**). Moreover, *LMO2*-  
179 knockdown in tumor-bearing mice led to a significantly reduced number of circulating  
180 tumor cells compared to control mice ( $P < 0.0001$ , ANOVA; **Fig. 2D**), implicating *LMO2*  
181 in tumor cell shedding, a key step in metastasis initiation. To extend our findings to  
182 more clinically relevant models, we used patient-derived xenograft (PDX) models  
183 previously generated in our lab (Sikandar et al., 2017). Consistent with our MDA-MB-  
184 468 studies, knockdown of *LMO2* dramatically decreased metastasis to the lung in three  
185 different PDX models of breast cancer (**Fig. 3E, F**), but did not significantly impact  
186 tumor growth (**Fig. S5B-D**).

187 To better understand how *LMO2* affects metastasis, we rigorously studied the effects of  
188 *LMO2* knockdown *in vitro* in MDA-MB-468 cells. Knockdown of *LMO2* showed  
189 significant impairment in the ability of cancer cells to migrate across transwells and  
190 invade through a 3D hydrogel matrix (**Fig. S6A, B**). Importantly, since *LMO2*<sup>+</sup> epithelial  
191 cells associated with endothelial cells in patient samples, we tested whether knockdown  
192 of *LMO2* decreased this association in co-culture assays. We found that in 3D co-

193 culture assays with human vascular endothelial cells (HUVECs), LMO2 knockdown  
194 significantly impacted incorporation of cancer cells into HUVEC tubes (**Fig. S6C**). To  
195 confirm that the effects of knockdown were specific to LMO2, we overexpressed LMO2  
196 in cells with shRNA targeting the 3'UTR. We found that all phenotypes of migration (**Fig.**  
197 **3G**), invasion (**Fig. 3H**), and incorporation into the vasculature *in vitro* (**Fig. 3I**) could be  
198 rescued by overexpression of LMO2 in LMO2-deficient cells. Lastly, to test whether  
199 LMO2 is required after metastatic cells enter circulation, we injected control and LMO2  
200 knockdown cells into the tail vein. We found that LMO2 knockdown did not significantly  
201 impact the formation of lung metastases when cells were directly injected in the tail vein,  
202 suggesting that LMO2 is critical for the initial dissemination of cancer cells from the  
203 tumor, but not extravasation and formation of metastatic foci (**Fig. S6D**).

204 **RNA sequencing identifies LMO2 as a regulator of IL6-JAK-STAT3 signaling.**  
205 To elucidate the molecular function of LMO2 in breast cancer cells, we performed bulk  
206 RNA sequencing of MDA-MB-468 cells after transfection with control and LMO2 shRNA  
207 vectors (**Fig. 4A**). Among the top 50 genes downregulated after LMO2 knockdown were  
208 genes previously implicated in metastasis, such as *BMP2* (Bach et al., 2018; Huang et  
209 al., 2017; Wang et al., 2017), *LGR6* (Leushacke and Barker, 2012; Ruan et al., 2019),  
210 *EGR4* (Matsuo et al., 2014), *TDO2* (D'Amato et al., 2015) and *S100A4* (Boye and  
211 Maelandsmo, 2010; Garrett et al., 2006; Helfman et al., 2005) (**Fig. 4A, Table S4**).  
212 Using Gene Set Enrichment Analysis (GSEA) (Mootha et al., 2003; Subramanian et al.,  
213 2005), we found that inflammatory pathways, such as  $\text{TNF}\alpha$  via NF- $\kappa$ B signaling, IL6-  
214 JAK-STAT3 signaling, and  $\text{IFN}\gamma$  response, were significantly downregulated in LMO2  
215 knockdown as compared to control conditions (**Fig. 4B**). To confirm our findings in  
216 primary patient samples we performed single-sample GSEA in our scRNA-seq data set  
217 as well as a larger published dataset of primary human breast cancer cells (Kim et al.,  
218 2018). We found that IL6-JAK-STAT3 signaling was significantly enriched in *LMO2<sup>+</sup>*  
219 versus *LMO2<sup>-</sup>* single cells (**Fig. 4C**) compared to other pathways (**Fig. S7**). In the  
220 hematopoietic system, LMO2 is an adaptor protein that facilitates formation of functional  
221 protein complexes which then activate transcription of downstream targets (Chambers  
222 and Rabitts, 2015). Hence, we asked whether LMO2 may similarly behave as a

223 bridging molecule to drive downstream signaling in breast epithelial cells. Using  
224 proximity ligation assays, we found that LMO2 had a significantly high binding affinity to  
225 STAT3, but not to NF- $\kappa$ B, further confirming our pathway analysis (**Fig. 4D**).

226 **LMO2 is required for STAT3 activation by IL6 and TNF $\alpha$ .**

227 To demonstrate specificity and functional significance of the LMO2-STAT3 interaction,  
228 we first showed that LMO2 knockdown significantly reduced LMO2-STAT3 binding ( $P <$   
229 0.0001, ANOVA; **Fig. 5A**). We also confirmed the LMO2-STAT3 interaction using co-  
230 immunoprecipitation assays (Co-IP) of LMO2 with STAT3 (**Fig. 5B**) and, a reverse Co-  
231 IP of STAT3 with LMO2 (**Fig. 5C**). In breast cancer, STAT3 is activated by cytokines,  
232 such as IL6 (Zhong et al., 1994), TNF $\alpha$  (De Simone et al., 2015), IFN $\alpha$  (Beadling et al.,  
233 1994; Cho et al., 1996; Darnell et al., 1994) and IFN $\gamma$  (Darnell et al., 1994; Will et al.,  
234 1996), as well as receptor tyrosine kinases such as EGFR (Kim et al., 2012; Zhao et al.,  
235 2020), leading to phosphorylation of STAT3. Dimerization of pSTAT3 and translocation  
236 to the nucleus activates transcription of downstream target genes involved in several  
237 processes, including metastasis. To understand whether the STAT3-LMO2 interaction  
238 has an effect on downstream STAT3 signaling, we used a STAT3-luciferase reporter  
239 assay. We stimulated control or LMO2 knockdown cells with IL6, TNF $\alpha$ , IFN $\gamma$ , IFN $\alpha$ , and  
240 EGF. We found that cells with knockdown of LMO2 were unable to induce transcription  
241 of the STAT3-luciferase reporter when treated with IL6 and TNF $\alpha$  as compared to  
242 control (**Fig. 5D**), but STAT3-luciferase was activated by IFN $\gamma$ , IFN $\alpha$ , and EGFR  
243 treatment. This suggests that LMO2 function in breast cancer cells is specific to  
244 activation of STAT3 signaling through IL6 and TNF $\alpha$ . On a molecular level, we found  
245 that knockdown of LMO2 significantly reduced STAT3 phosphorylation at Tyr705, which  
246 is required for its dimerization and transcriptional activity (**Fig. 5E and Fig. S8**). To  
247 understand how LMO2 regulates phosphorylation of STAT3, we examined the  
248 interaction of STAT3 with its upstream activator JAK2 and its cytoplasmic inhibitor  
249 PIAS3. Knockdown of LMO2 decreased the interaction of STAT3 with JAK2 (**Fig. 5F**)  
250 and allowed for increased interaction with its inhibitor, PIAS3 (**Fig. 5G**). This suggests  
251 that LMO2 works as an adaptor protein in the cytoplasm to stabilize the STAT3-JAK2  
252 interaction, thereby allowing efficient phosphorylation and activation of STAT3 while

253 simultaneously preventing its negative regulation by PIAS3 (**Fig. 5H**). This LMO2-  
254 mediated control of a core inflammatory response pathway could enable cancer cells to  
255 rapidly transition between cellular phenotypes required for metastasis and represents a  
256 therapeutic vulnerability that could be targeted.

257 **DISCUSSION**

258 Efficient metastasis of tumor cells requires transition from a proliferative to an invasive  
259 state and back to a proliferative state at a distant site (Beerling et al., 2016). Previous  
260 studies using mouse tumor models have demonstrated the requirement of a basal  
261 epithelial program in metastasis (Cheung et al., 2013; Padmanaban et al., 2019) and  
262 showed that hybrid epithelial-mesenchymal states (Beerling et al., 2016; Kröger et al.,  
263 2019; Nieto et al., 2016) in metastasis express angiogenic factors (Pastushenko et al.,  
264 2018). Here, we have identified a population of *THY1<sup>+</sup>/VEGFA<sup>+</sup>* human basal epithelial  
265 cells with higher transcriptional diversity that is marked by transient expression of  
266 *LMO2*. Moreover, we demonstrate that *Lmo2* lineage-traced epithelial cells have a  
267 higher propensity to form lung metastases. Moreover, knockdown of *LMO2* decreases  
268 lung metastasis in multiple tumor models of human breast cancer by affecting multiple  
269 steps during intravasation. It is important to note that only a subset of *Lmo2* lineage-  
270 traced cells show vascular phenotypes, suggesting specific epigenetic regulation that is  
271 activated in the presence of TNF $\alpha$  and IL6 from the microenvironment. Our observations  
272 highlight a heterogenous, cancer-cell-intrinsic response to the microenvironment while  
273 previous studies have demonstrated that there is a reciprocal effect of cancer cells on  
274 the tumor microenvironment with recruitment of macrophages and cross-talk with tumor  
275 endothelial cells during metastasis (Borriello et al., 2020).

276 *LMO2* has been extensively studied in hematological malignancies and is well-  
277 established as a transcriptional adaptor protein (Chambers and Rabbitts, 2015). Recent  
278 studies have attempted to understand the role of *LMO2* in breast cancer (Hu et al.,  
279 2021; Liu et al., 2016; Liu et al., 2017) but have suffered from contradictory results,  
280 were limited to cell lines, and did not attribute *LMO2* to any particular tumor cell  
281 population. We demonstrate that *LMO2* is a previously unidentified binding partner of

282 STAT3 in breast cancer cells and modulates STAT3 signaling in response to IL6 and  
283 TNF $\alpha$ . We speculate that the expression of LMO2 provides the necessary threshold to  
284 stabilize STAT3 signaling, which in turn enables the tumor cells to enter a transient  
285 metastatic state (Wendt et al., 2014) and escape the primary tumor. STAT3 signaling is  
286 involved in a number of processes and its targets may be defined in unison with other  
287 contextual signals such as inflammation. Several studies have linked low chronic  
288 inflammation in cancer to metastasis (Joyce and Pollard, 2009; Liu et al., 2015). We  
289 speculate that LMO2 is a critical molecular link between these processes and define a  
290 novel function for LMO2 in breast cancer metastasis. The development of new methods  
291 targeting adaptor proteins (Wang et al., 2020) and small molecules that disrupt the  
292 LMO2-STAT3 axis (Milton-Harris et al., 2020) could provide novel therapeutic strategies  
293 to modulate STAT3 signaling and inhibit metastatic colonization in breast cancer.

294 **REFERENCES AND NOTES**

- 295 Al-Hajj, M., Wicha, M.S., Benito-Hernandez, A., Morrison, S.J., and Clarke, M.F. (2003).  
296 Prospective identification of tumorigenic breast cancer cells. *Proc Natl Acad Sci U S A*  
297 100, 3983-3988.
- 298 Bach, D.H., Park, H.J., and Lee, S.K. (2018). The Dual Role of Bone Morphogenetic  
299 Proteins in Cancer. *Mol Ther Oncolytics* 8, 1-13.
- 300 Beadling, C., Guschin, D., Witthuhn, B.A., Ziemiecki, A., Ihle, J.N., Kerr, I.M., and  
301 Cantrell, D.A. (1994). Activation of JAK kinases and STAT proteins by interleukin-2 and  
302 interferon alpha, but not the T cell antigen receptor, in human T lymphocytes. *EMBO J*  
303 13, 5605-5615.
- 304 Beerling, E., Seinstra, D., de Wit, E., Kester, L., van der Velden, D., Maynard, C.,  
305 Schäfer, R., van Diest, P., Voest, E., van Oudenaarden, A., *et al.* (2016). Plasticity  
306 between Epithelial and Mesenchymal States Unlinks EMT from Metastasis-Enhancing  
307 Stem Cell Capacity. *Cell Reports* 14, 2281-2288.
- 308 Borriello, L., Karagiannis, G.S., Duran, C.L., Coste, A., Oktay, M.H., Entenberg, D., and  
309 Condeelis, J.S. (2020). The role of the tumor microenvironment in tumor cell  
310 intravasation and dissemination. *European Journal of Cell Biology* 99, 151098.
- 311 Boye, K., and Maelandsmo, G.M. (2010). S100A4 and metastasis: a small actor playing  
312 many roles. *Am J Pathol* 176, 528-535.
- 313 Chambers, J., and Rabbitts, T.H. (2015). LMO2 at 25 years: a paradigm of  
314 chromosomal translocation proteins. *Open Biol* 5, 150062-150062.
- 315 Cheung, K.J., Gabrielson, E., Werb, Z., and Ewald, A.J. (2013). Collective invasion in  
316 breast cancer requires a conserved basal epithelial program. *Cell* 155, 1639-1651.
- 317 Cho, R.W., Wang, X., Diehn, M., Shedd, K., Chen, G.Y., Sherlock, G., Gurney, A.,  
318 Lewicki, J., and Clarke, M.F. (2008). Isolation and Molecular Characterization of Cancer  
319 Stem Cells in MMTV-Wnt-1 Murine Breast Tumors. *STEM CELLS* 26, 364-371.
- 320 Cho, S.S., Bacon, C.M., Sudarshan, C., Rees, R.C., Finbloom, D., Pine, R., and  
321 O'Shea, J.J. (1996). Activation of STAT4 by IL-12 and IFN-alpha: evidence for the  
322 involvement of ligand-induced tyrosine and serine phosphorylation. *J Immunol* 157,  
323 4781-4789.
- 324 Curtis, C., Shah, S.P., Chin, S.F., Turashvili, G., Rueda, O.M., Dunning, M.J., Speed,  
325 D., Lynch, A.G., Samarajiwa, S., Yuan, Y., *et al.* (2012). The genomic and  
326 transcriptomic architecture of 2,000 breast tumours reveals novel subgroups. *Nature*  
327 486, 346-352.
- 328 D'Amato, N.C., Rogers, T.J., Gordon, M.A., Greene, L.I., Cochrane, D.R., Spoelstra,  
329 N.S., Nemkov, T.G., D'Alessandro, A., Hansen, K.C., and Richer, J.K. (2015). A TDO2-  
330 AhR signaling axis facilitates anoikis resistance and metastasis in triple-negative breast  
331 cancer. *Cancer Res* 75, 4651-4664.
- 332 Darnell, J.E., Jr., Kerr, I.M., and Stark, G.R. (1994). Jak-STAT pathways and  
333 transcriptional activation in response to IFNs and other extracellular signaling proteins.  
334 *Science* 264, 1415-1421.
- 335 De Simone, V., Franze, E., Ronchetti, G., Colantoni, A., Fantini, M.C., Di Fusco, D.,  
336 Sica, G.S., Sileri, P., MacDonald, T.T., Pallone, F., *et al.* (2015). Th17-type cytokines,  
337 IL-6 and TNF-alpha synergistically activate STAT3 and NF-kB to promote colorectal  
338 cancer cell growth. *Oncogene* 34, 3493-3503.

- 339 Esposito, M., Ganesan, S., and Kang, Y. (2021). Emerging strategies for treating  
340 metastasis. *Nature Cancer* 2, 258-270.
- 341 Esserman, L.J., Berry, D.A., Cheang, M.C., Yau, C., Perou, C.M., Carey, L., DeMichele,  
342 A., Gray, J.W., Conway-Dorsey, K., Lenburg, M.E., *et al.* (2012). Chemotherapy  
343 response and recurrence-free survival in neoadjuvant breast cancer depends on  
344 biomarker profiles: results from the I-SPY 1 TRIAL (CALGB 150007/150012; ACRIN  
345 6657). *Breast Cancer Res Treat* 132, 1049-1062.
- 346 Fischer, K.R., Durrans, A., Lee, S., Sheng, J., Li, F., and Wong, S.T. (2015). Epithelial-  
347 to-mesenchymal transition is not required for lung metastasis but contributes to  
348 chemoresistance. *Nature* 527.
- 349 Garrett, S.C., Varney, K.M., Weber, D.J., and Bresnick, A.R. (2006). S100A4, a  
350 mediator of metastasis. *J Biol Chem* 281, 677-680.
- 351 Gratzinger, D., Zhao, S., West, R., Rouse, R.V., Vogel, H., Gil, E.C., Levy, R., Lossos,  
352 I.S., and Natkunam, Y. (2009). The transcription factor LMO2 is a robust marker of  
353 vascular endothelium and vascular neoplasms and selected other entities. *Am J Clin  
354 Pathol* 131, 264-278.
- 355 Gulati, G.S., Sikandar, S.S., Wesche, D.J., Manjunath, A., Bharadwaj, A., Berger, M.J.,  
356 Ilagan, F., Kuo, Angera H., Hsieh, R.W., Cai, S., *et al.* (2020). Single-cell transcriptional  
357 diversity is a hallmark of developmental potential. *Science* 367, 405-411.
- 358 Guy, C.T., Cardiff, R.D., and Muller, W.J. (1992). Induction of mammary tumors by  
359 expression of polyomavirus middle T oncogene: a transgenic mouse model for  
360 metastatic disease. *Molecular and Cellular Biology* 12, 954-961.
- 361 Helfman, D.M., Kim, E.J., Lukanidin, E., and Grigorian, M. (2005). The metastasis  
362 associated protein S100A4: role in tumour progression and metastasis. *Br J Cancer* 92,  
363 1955-1958.
- 364 Herschkowitz, J.I., Simin, K., Weigman, V.J., Mikaelian, I., Usary, J., Hu, Z.,  
365 Rasmussen, K.E., Jones, L.P., Assefnia, S., Chandrasekharan, S., *et al.* (2007).  
366 Identification of conserved gene expression features between murine mammary  
367 carcinoma models and human breast tumors. *Genome Biology* 8, R76.
- 368 Hu, A., Hong, F., Li, D., Xie, Q., Chen, K., Zhu, L., and He, H. (2021). KDM3B-ETF1  
369 fusion gene downregulates LMO2 via the WNT/β-catenin signaling pathway, promoting  
370 metastasis of invasive ductal carcinoma. *Cancer Gene Therapy*.
- 371 Huang, P., Chen, A., He, W., Li, Z., Zhang, G., Liu, Z., Liu, G., Liu, X., He, S., Xiao, G.,  
372 *et al.* (2017). BMP-2 induces EMT and breast cancer stemness through Rb and CD44.  
373 *Cell Death Discov* 3, 17039.
- 374 Joyce, J.A., and Pollard, J.W. (2009). Microenvironmental regulation of metastasis.  
375 *Nature reviews Cancer* 9, 239-252.
- 376 Kim, C., Gao, R., Sei, E., Brandt, R., Hartman, J., Hatschek, T., Crosetto, N., Foukakis,  
377 T., and Navin, N.E. (2018). Chemoresistance Evolution in Triple-Negative Breast  
378 Cancer Delineated by Single-Cell Sequencing. *Cell* 173, 879-893.e813.
- 379 Kim, S.M., Kwon, O.J., Hong, Y.K., Kim, J.H., Solca, F., Ha, S.J., Soo, R.A.,  
380 Christensen, J.G., Lee, J.H., and Cho, B.C. (2012). Activation of IL-6R/JAK1/STAT3  
381 signaling induces de novo resistance to irreversible EGFR inhibitors in non-small cell  
382 lung cancer with T790M resistance mutation. *Mol Cancer Ther* 11, 2254-2264.
- 383 Kröger, C., Afeyan, A., Mraz, J., Eaton, E.N., Reinhardt, F., Khodor, Y.L., Thiru, P.,  
384 Bierie, B., Ye, X., Burge, C.B., *et al.* (2019). Acquisition of a hybrid E/M state is

- 385 essential for tumorigenicity of basal breast cancer cells. *Proceedings of the National*  
386 *Academy of Sciences of the United States of America* **116**, 7353-7362.
- 387 Larson, R.C., Osada, H., Larson, T.A., Lavenir, I. & Rabbitts, T.H (1995). The oncogenic  
388 LIM protein Rbtn2 causes thymic developmental aberrations that precede malignancy in  
389 transgenic mice. *Oncogene* **11**, 853-862.
- 390 Lawson, D.A., Kessenbrock, K., Davis, R.T., Pervolarakis, N., and Werb, Z. (2018).  
391 Tumour heterogeneity and metastasis at single-cell resolution. *Nat Cell Biol* **20**, 1349-  
392 1360.
- 393 Leushacke, M., and Barker, N. (2012). Lgr5 and Lgr6 as markers to study adult stem  
394 cell roles in self-renewal and cancer. *Oncogene* **31**, 3009-3022.
- 395 Li, Y., Lv, Z., Zhang, S., Wang, Z., He, L., Tang, M., Pu, W., Zhao, H., Zhang, Z., Shi,  
396 Q., *et al.* (2020). Genetic Fate Mapping of Transient Cell Fate Reveals N-Cadherin  
397 Activity and Function in Tumor Metastasis. *Dev Cell* **54**, 593-607.e595.
- 398 Liu, H., Patel, M.R., Prescher, J.A., Patsialou, A., Qian, D., Lin, J., Wen, S., Chang, Y.-  
399 F., Bachmann, M.H., Shimono, Y., *et al.* (2010). Cancer stem cells from human breast  
400 tumors are involved in spontaneous metastases in orthotopic mouse models.  
401 *Proceedings of the National Academy of Sciences* **107**, 18115-18120.
- 402 Liu, J., Lin, P.C., and Zhou, B.P. (2015). Inflammation fuels tumor progress and  
403 metastasis. *Curr Pharm Des* **21**, 3032-3040.
- 404 Liu, Y., Huang, D., Wang, Z., Wu, C., Zhang, Z., Wang, D., Li, Z., Zhu, T., Yang, S., and  
405 Sun, W. (2016). LMO2 attenuates tumor growth by targeting the Wnt signaling pathway  
406 in breast and colorectal cancer. *Sci Rep* **6**, 36050-36050.
- 407 Liu, Y., Wang, Z., Huang, D., Wu, C., Li, H., Zhang, X., Meng, B., Li, Z., Zhu, T., Yang,  
408 S., *et al.* (2017). LMO2 promotes tumor cell invasion and metastasis in basal-type  
409 breast cancer by altering actin cytoskeleton remodeling. *Oncotarget* **8**, 9513-9524.
- 410 Lobo, N.A., Zabala, M., Qian, D., and Clarke, M.F. (2018). Serially transplantable  
411 mammary epithelial cells express the Thy-1 antigen. *Breast Cancer Res* **20**, 121-121.
- 412 Lu, W., and Kang, Y. (2019). Epithelial-Mesenchymal Plasticity in Cancer Progression  
413 and Metastasis. *Dev Cell* **49**, 361-374.
- 414 Matsuo, T., Dat le, T., Komatsu, M., Yoshimaru, T., Daizumoto, K., Sone, S., Nishioka,  
415 Y., and Katagiri, T. (2014). Early growth response 4 is involved in cell proliferation of  
416 small cell lung cancer through transcriptional activation of its downstream genes. *PLoS*  
417 *one* **9**, e113606.
- 418 Mercurio, A.M., Lipscomb, E.A., and Bachelder, R.E. (2005). Non-Angiogenic Functions  
419 of VEGF in Breast Cancer. *Journal of Mammary Gland Biology and Neoplasia* **10**, 283-  
420 290.
- 421 Milton-Harris, L., Jeeves, M., Walker, S.A., Ward, S.E., and Mancini, E.J. (2020). Small  
422 molecule inhibits T-cell acute lymphoblastic leukaemia oncogenic interaction through  
423 conformational modulation of LMO2. *Oncotarget*; Vol 11, No 19.
- 424 Mootha, V.K., Lindgren, C.M., Eriksson, K.F., Subramanian, A., Sihag, S., Lehar, J.,  
425 Puigserver, P., Carlsson, E., Ridderstrale, M., Laurila, E., *et al.* (2003). PGC-1alpha-  
426 responsive genes involved in oxidative phosphorylation are coordinately downregulated  
427 in human diabetes. *Nat Genet* **34**, 267-273.
- 428 Newman, A.M., Steen, C.B., Liu, C.L., Gentles, A.J., Chaudhuri, A.A., Scherer, F.,  
429 Khodadoust, M.S., Esfahani, M.S., Luca, B.A., Steiner, D., *et al.* (2019). Determining

- 430 cell type abundance and expression from bulk tissues with digital cytometry. *Nature Biotechnology* 37, 773-782.
- 431
- 432 Nieto, M.A., Huang, R.Y., Jackson, R.A., and Thiery, J.P. (2016). Emt: 2016. *Cell* 166, 21-45.
- 433
- 434 Padmanaban, V., Krol, I., Suhail, Y., Szczerba, B.M., Aceto, N., Bader, J.S., and Ewald, A.J. (2019). E-cadherin is required for metastasis in multiple models of breast cancer. *Nature* 573, 439-444.
- 435
- 436
- 437 Pastushenko, I., Brisebarre, A., Sifrim, A., Fioramonti, M., Revenco, T., Boumahdi, S., Van Keymeulen, A., Brown, D., Moers, V., Lemaire, S., *et al.* (2018). Identification of the tumour transition states occurring during EMT. *Nature* 556, 463-468.
- 438
- 439
- 440 Pastushenko, I., Mauri, F., Song, Y., de Cock, F., Meeusen, B., Swedlund, B., Impens, F., Van Haver, D., Opitz, M., Thery, M., *et al.* (2021). Fat1 deletion promotes hybrid EMT state, tumour stemness and metastasis. *Nature* 589, 448-455.
- 441
- 442
- 443 Perou, C.M., Sørlie, T., Eisen, M.B., van de Rijn, M., Jeffrey, S.S., Rees, C.A., Pollack, J.R., Ross, D.T., Johnsen, H., Akslen, L.A., *et al.* (2000). Molecular portraits of human breast tumours. *Nature* 406, 747-752.
- 444
- 445
- 446 Rios, A.C., Fu, N.Y., Lindeman, G.J., and Visvader, J.E. (2014). In situ identification of bipotent stem cells in the mammary gland. *Nature* 506, 322-327.
- 447
- 448 Ruan, X., Liu, A., Zhong, M., Wei, J., Zhang, W., Rong, Y., Liu, W., Li, M., Qing, X., Chen, G., *et al.* (2019). Silencing LGR6 Attenuates Stemness and Chemoresistance via Inhibiting Wnt/β-Catenin Signaling in Ovarian Cancer. *Molecular therapy oncolytics* 14, 94-106.
- 449
- 450
- 451
- 452 Shen, M., and Kang, Y. (2019). Role Reversal: A Pro-metastatic Function of E-Cadherin. *Dev Cell* 51, 417-419.
- 453
- 454 Siegel, R., Ward, E., Brawley, O., and Jemal, A. (2011). Cancer statistics, 2011. *CA: A Cancer Journal for Clinicians* 61, 212-236.
- 455
- 456 Siegel, R.L., Miller, K.D., Fuchs, H.E., and Jemal, A. (2021). Cancer Statistics, 2021. *CA: A Cancer Journal for Clinicians* 71, 7-33.
- 457
- 458 Sikandar, S.S., Kuo, A.H., Kalisky, T., Cai, S., Zabala, M., Hsieh, R.W., Lobo, N.A., Scheeren, F.A., Sim, S., Qian, D., *et al.* (2017). Role of epithelial to mesenchymal transition associated genes in mammary gland regeneration and breast tumorigenesis. *Nature Communications* 8, 1669.
- 459
- 460
- 461
- 462 Subramanian, A., Tamayo, P., Mootha, V.K., Mukherjee, S., Ebert, B.L., Gillette, M.A., Paulovich, A., Pomeroy, S.L., Golub, T.R., Lander, E.S., *et al.* (2005). Gene set enrichment analysis: a knowledge-based approach for interpreting genome-wide expression profiles. *Proc Natl Acad Sci U S A* 102, 15545-15550.
- 463
- 464
- 465
- 466 Tanay, A., and Regev, A. (2017). Scaling single-cell genomics from phenomenology to mechanism. *Nature* 541, 331-338.
- 467
- 468 TCGA (2012). Comprehensive molecular portraits of human breast tumours. *Nature* 490, 61-70.
- 469
- 470 van Amerongen, R., Bowman, A.N., and Nusse, R. (2012). Developmental stage and time dictate the fate of Wnt/beta-catenin-responsive stem cells in the mammary gland. *Cell Stem Cell* 11, 387-400.
- 471
- 472
- 473 Van Keymeulen, A., Rocha, A.S., Ousset, M., Beck, B., Bouvencourt, G., Rock, J., Sharma, N., Dekoninck, S., and Blanpain, C. (2011). Distinct stem cells contribute to mammary gland development and maintenance. *Nature* 479, 189-193.
- 474
- 475

- 476 Wang, M.H., Zhou, X.M., Zhang, M.Y., Shi, L., Xiao, R.W., Zeng, L.S., Yang, X.Z.,  
477 Zheng, X.F.S., Wang, H.Y., and Mai, S.J. (2017). BMP2 promotes proliferation and  
478 invasion of nasopharyngeal carcinoma cells via mTORC1 pathway. *Aging (Albany NY)*  
479 9, 1326-1340.
- 480 Wang, Y., Jiang, X., Feng, F., Liu, W., and Sun, H. (2020). Degradation of proteins by  
481 PROTACs and other strategies. *Acta Pharm Sin B* 10, 207-238.
- 482 Wendt, M.K., Balanis, N., Carlin, C.R., and Schiemann, W.P. (2014). STAT3 and  
483 epithelial-mesenchymal transitions in carcinomas. *JAKSTAT* 3, e28975.
- 484 Will, A., Hemmann, U., Horn, F., Rollinghoff, M., and Gessner, A. (1996). Intracellular  
485 murine IFN-gamma mediates virus resistance, expression of oligoadenylyate synthetase,  
486 and activation of STAT transcription factors. *J Immunol* 157, 4576-4583.
- 487 Yamada, Y., Warren, A.J., Dobson, C., Forster, A., Pannell, R., and Rabitts, T.H.  
488 (1998). The T cell leukemia LIM protein Lmo2 is necessary for adult mouse  
489 hematopoiesis. *Proceedings of the National Academy of Sciences of the United States  
490 of America* 95, 3890-3895.
- 491 Ye, X., Brabletz, T., Kang, Y., Longmore, G.D., Nieto, M.A., Stanger, B.Z., Yang, J., and  
492 Weinberg, R.A. (2017). Upholding a role for EMT in breast cancer metastasis. *Nature*  
493 547, E1-E3.
- 494 Zhao, C., Yang, L., Zhou, F., Yu, Y., Du, X., Xiang, Y., Li, C., Huang, X., Xie, C., Liu, Z.,  
495 et al. (2020). Feedback activation of EGFR is the main cause for STAT3 inhibition-  
496 irresponsiveness in pancreatic cancer cells. *Oncogene* 39, 3997-4013.
- 497 Zhao, D., Pan, C., Sun, J., Gilbert, C., Drews-Elger, K., Azzam, D.J., Picon-Ruiz, M.,  
498 Kim, M., Ullmer, W., El-Ashry, D., et al. (2015). VEGF drives cancer-initiating stem cells  
499 through VEGFR-2/Stat3 signaling to upregulate Myc and Sox2. *Oncogene* 34, 3107-  
500 3119.
- 501 Zhong, Z., Wen, Z., and Darnell, J.E., Jr. (1994). Stat3: a STAT family member  
502 activated by tyrosine phosphorylation in response to epidermal growth factor and  
503 interleukin-6. *Science* 264, 95-98.

504 **ACKNOWLEDGMENTS**

505 We thank Patricia Lovelace, Catherine Carswell Crumpton, and other flow cytometry  
506 staff for their help and animal facility core members. The Wolverine Aria instrument was  
507 funded by NHI grant S10-1S10RR02933801. We thank Diane Heiser for technical  
508 assistance with the tail vein injections. We thank Margaret Cuadro for administrative  
509 assistance. We thank the Stanford Neuroscience Microscopy Service, supported by NIH  
510 grant NS069375.

511 **Funding:** This work was supported by NIH/NCI (U01CA154209-01 and P01 CA139490-  
512 05), the Breast Cancer Research Foundation (to M.F.C.), the U.S. Department of  
513 Defense (W81XWH-11-1-0287 and W81XWH-13-1-0281 to M.F.C.; S.S.S., W81XWH-  
514 12-1-0020), the National Cancer Institute (A.M.N., R00CA187192-03; M.F.C.,  
515 5R01CA100225-09; G.S.G., PHS grant no. CA09302), the Stanford Bio-X  
516 Interdisciplinary Initiatives Seed Grants Program (IIP) (A.M.N., M.F.C.), the Virginia and  
517 D.K. Ludwig Fund for Cancer Research (A.M.N., M.F.C), the Stinehart-Reed Foundation  
518 (A.M.N.), the Stanford School of Medicine Dean's Fellowship (J.A.), Stanford Bio-X  
519 Bowes Graduate Student Fellowship (G.S.G.), and the Stanford Medical Science  
520 Training Program (G.S.G.). K.R-H. is a New York Stem Cell Foundation – Robertson  
521 Investigator. K.R-H. is also supported by the NIH (R01-HL128503)

522 **AUTHOR CONTRIBUTIONS**

523 S.S.S. and M.F.C. conceived and designed the study. S.S.S. and J.A. performed  
524 experiments and analyzed data with supervision from M.F.C. G.S.G. analyzed single-  
525 cell and bulk RNA sequencing data with assistance from C.B.S. and supervision from  
526 A.M.N. A.H.K. assisted with the PDX studies. W.H.D.H. assisted with the metastasis  
527 experiments. S.D. performed staining for visualization of tumor vasculature under the  
528 supervision of K.R-H. T.A.P. assisted with the circulating cells experiment under the  
529 supervision of P.B. D.Q. provided technical support. F.D. assisted with the collection of  
530 patient specimens. J.P.T. assessed the enrichment of genes in LMO2<sup>+</sup> cells and  
531 provided guidance in the project. T.R provided the *Lmo2*<sup>CreERT2</sup> mice. S.S.S., J.A.,  
532 G.S.G., A.M.N. and M.F.C., wrote the manuscript. All authors commented on the  
533 manuscript.

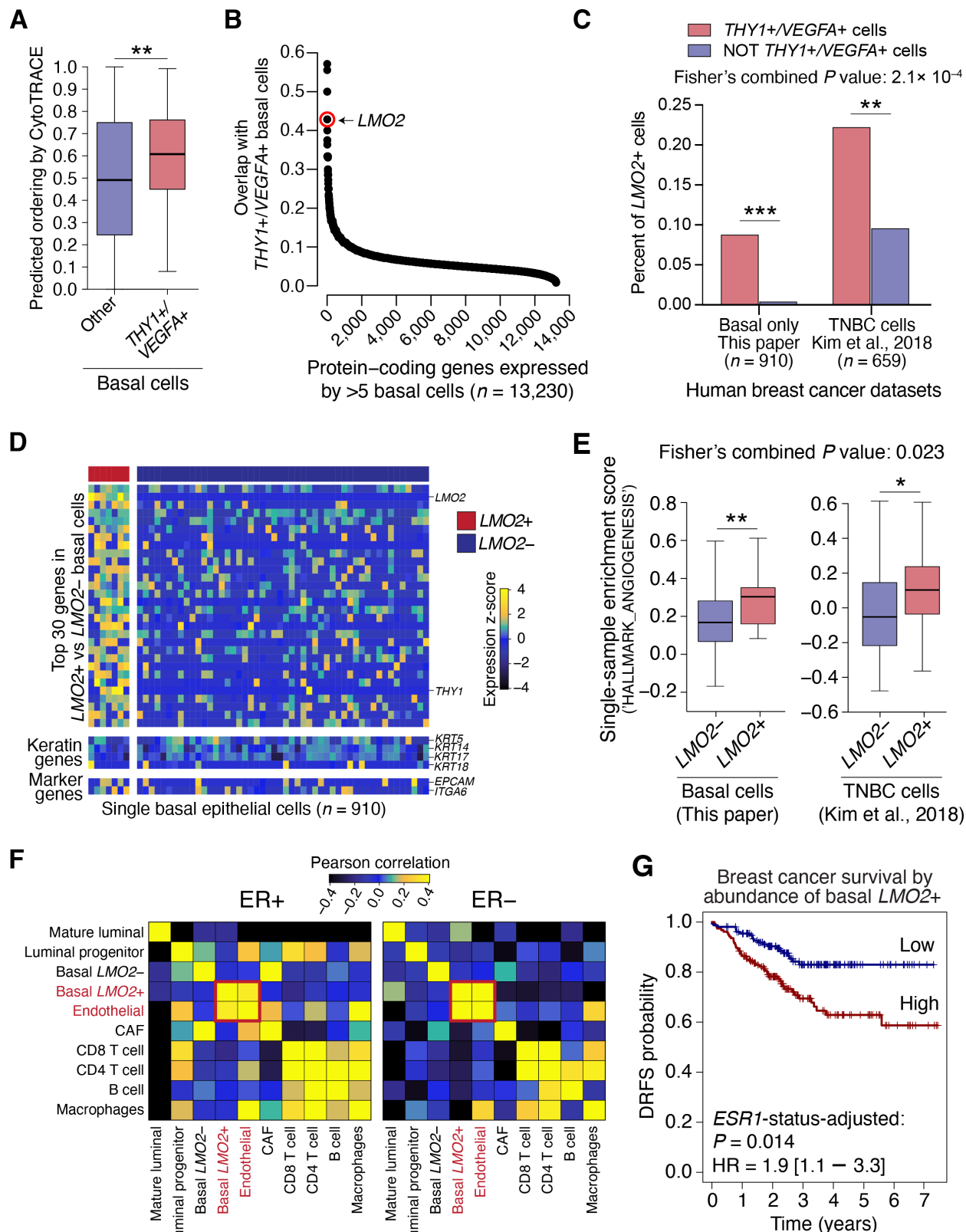
534 **Supplementary Materials:**

535 Materials and Methods

536 Figures S1-S8

537 Tables S1-S5

## Figures and Figure Legends



538 **Figure 1: Identification of an immature basal epithelial population associated with**  
539 **pro-angiogenic signaling and poor survival in human breast cancer.**

540 (A) Differentiation scores of basal epithelial cells from 17 human breast tumors profiled  
541 by scRNA-seq (all but 'SU196' contained basal cells). Differentiation scores were  
542 determined by CytoTRACE (Gulati et al., 2020). Statistical significance between *THY1*<sup>+</sup>/  
543 *VEGFA*<sup>+</sup> basal cells and other basal cells was calculated using an unpaired two-tailed *t*-  
544 test. \**P*<0.1; \*\**P*<0.05; \*\*\**P*<0.01.

545 (B) Plot showing protein-coding genes ordered by their enrichment in *THY1*<sup>+</sup>/*VEGFA*<sup>+</sup>  
546 basal cells from human breast tumors profiled by scRNA-seq. Enrichment was defined  
547 as the number of *THY1*<sup>+</sup>/*VEGFA*<sup>+</sup> basal cells expressing a given gene (TPM > 0)  
548 divided by the total number of cells expressing that gene. Only genes expressed by at  
549 least 5 basal cells were considered. *LMO2* is highlighted in red.

550 (C) Paired bar plots showing percent of *LMO2*<sup>+</sup> cells in *THY1*<sup>+</sup>/*VEGFA*<sup>+</sup> cells (red) and  
551 all other cells (blue) in two human breast cancer datasets, including Kim et al., 2018 (4  
552 primary triple-negative breast cancers, single nucleus RNA-sequencing, tumor only, *n* =  
553 659) (Kim et al., 2018), and the basal cells (see methods for details; *n* = 910) from this  
554 study. Statistical analysis was performed by Fisher's Exact Test for association of  
555 *LMO2*<sup>+</sup> cells with *THY1*<sup>+</sup>/*VEGFA*<sup>+</sup> cells. Individual and combined *P* values by Fisher's  
556 method are shown in the graph. \**P*<0.1; \*\**P*<0.05; \*\*\**P*<0.01.

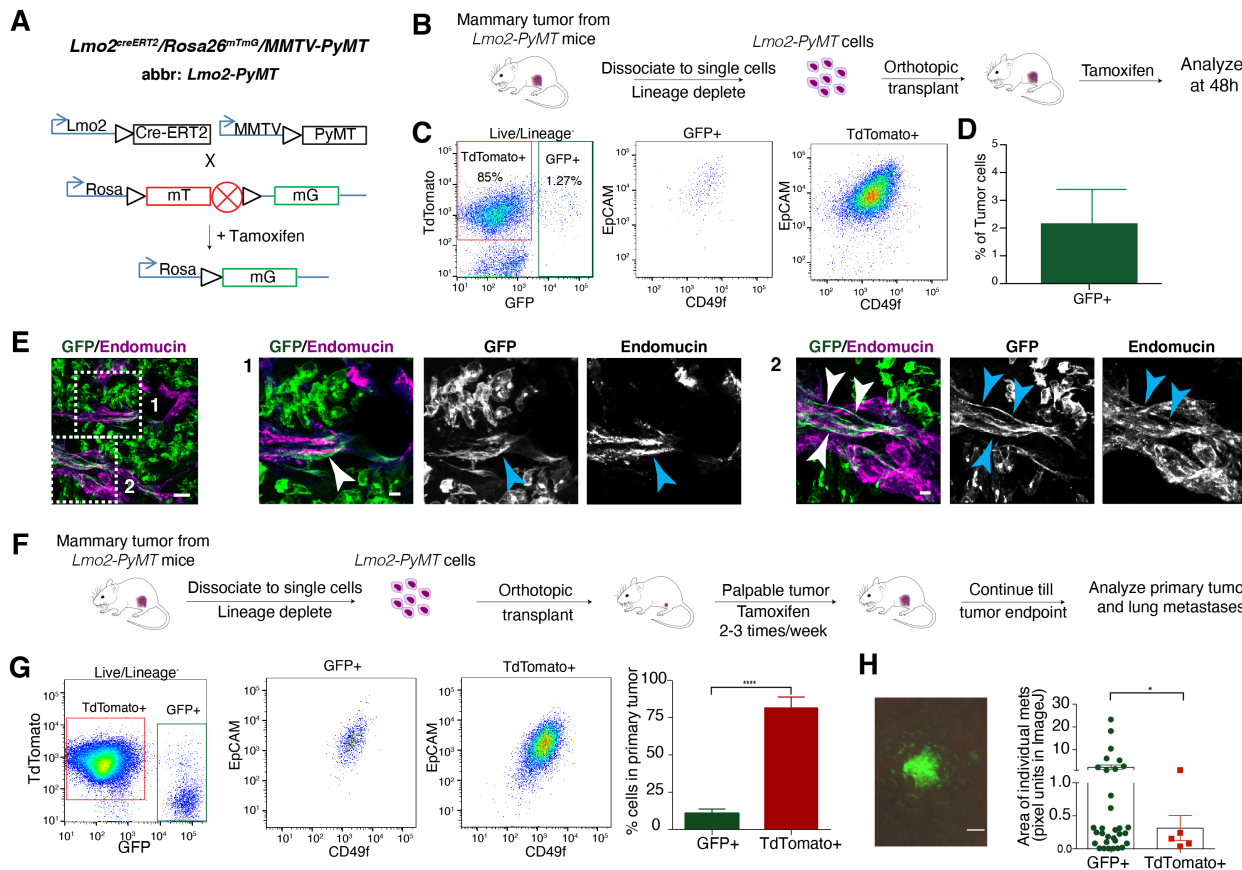
557 (D) Heatmap depicting the top 30 differentially expressed genes, along with selected  
558 keratin and lineage markers, in *LMO2*<sup>+</sup> (*n* = 7 cells) vs. *LMO2*<sup>-</sup> (*n* = 903 cells) basal  
559 epithelial cells from primary breast tumors. A random subsample of 50 *LMO2*<sup>-</sup> basal cell  
560 transcriptomes is shown for clarity. Color scale (above) represents z-score-normalized  
561 expression per gene.

562 (E) Differential enrichment of the 'HALLMARK\_ANGIOGENESIS' pathway in *LMO2*<sup>+</sup>  
563 vs. - in two independent human breast cancer datasets described in C. To ensure a fair  
564 comparison between *LMO2* positive and negative populations, an empirical *P* value was  
565 calculated by comparing the mean enrichment in *LMO2*<sup>+</sup> basal cells versus a size-  
566 matched collection of *LMO2*<sup>-</sup> basal cells randomly sampled 10,000 times. A combined *P*  
567 value by Fisher's method is also shown. \**P*<0.1; \*\**P*<0.05; \*\*\**P*<0.01.

568 (F and G) Cell-type and survival association of *LMO2*<sup>+</sup> basal cells across 508 bulk  
569 human breast tumor transcriptomes (Esserman et al., 2012) deconvolved using  
570 CIBERSORTx.

571 (F) Co-association patterns among cell type abundance profiles in bulk breast tumors,  
572 as quantified by Pearson correlation. Basal *LMO2*<sup>+</sup> cells and endothelial cells are  
573 highlighted.

574 (G) Kaplan Meier curves showing differences in distant recurrence-free survival (DRFS)  
575 in 508 breast cancer patients stratified by the median abundance of *LMO2*<sup>+</sup> basal  
576 epithelial cells. DRFS was modeled as a function of *LMO2*<sup>+</sup> basal cell status and *ESR1*  
577 status (**Methods**). The adjusted log-rank *P* value and hazard ratio with 95% confidence  
578 interval for *LMO2*<sup>+</sup> basal cell status is shown.



579 **Figure 2: *Lmo2* lineage-traced tumor epithelial cells integrate into the vasculature  
580 and can form metastasis in *PyMT* tumors.**

581 (A) Schematic diagram showing generation of the triple transgenic *Rosa26*<sup>mTmG</sup> reporter  
582 with *MMTV-PyMT* and *Lmo2-CreERT2* mice (referred to as *Lmo2-PyMT*).

583 (B) Schematic diagram showing the experimental scheme for *Lmo2-PyMT* tumors  
584 treated with tamoxifen.

585 (C) *Panel 1*: FACS analysis of *Lmo2-PyMT* tumors 48h after Tamoxifen pulse. Cells are  
586 gated on lineage<sup>-</sup> (CD45<sup>-</sup>, CD31<sup>-</sup>, Ter119<sup>-</sup>), DAPI<sup>-</sup> cells (See **Fig. S2**) and analyzed  
587 using TdTomato<sup>+</sup> and GFP<sup>+</sup>. *Panels 2 and 3*: EpCAM and CD49f expression status in  
588 GFP<sup>+</sup> and TdTomato<sup>+</sup> cells.

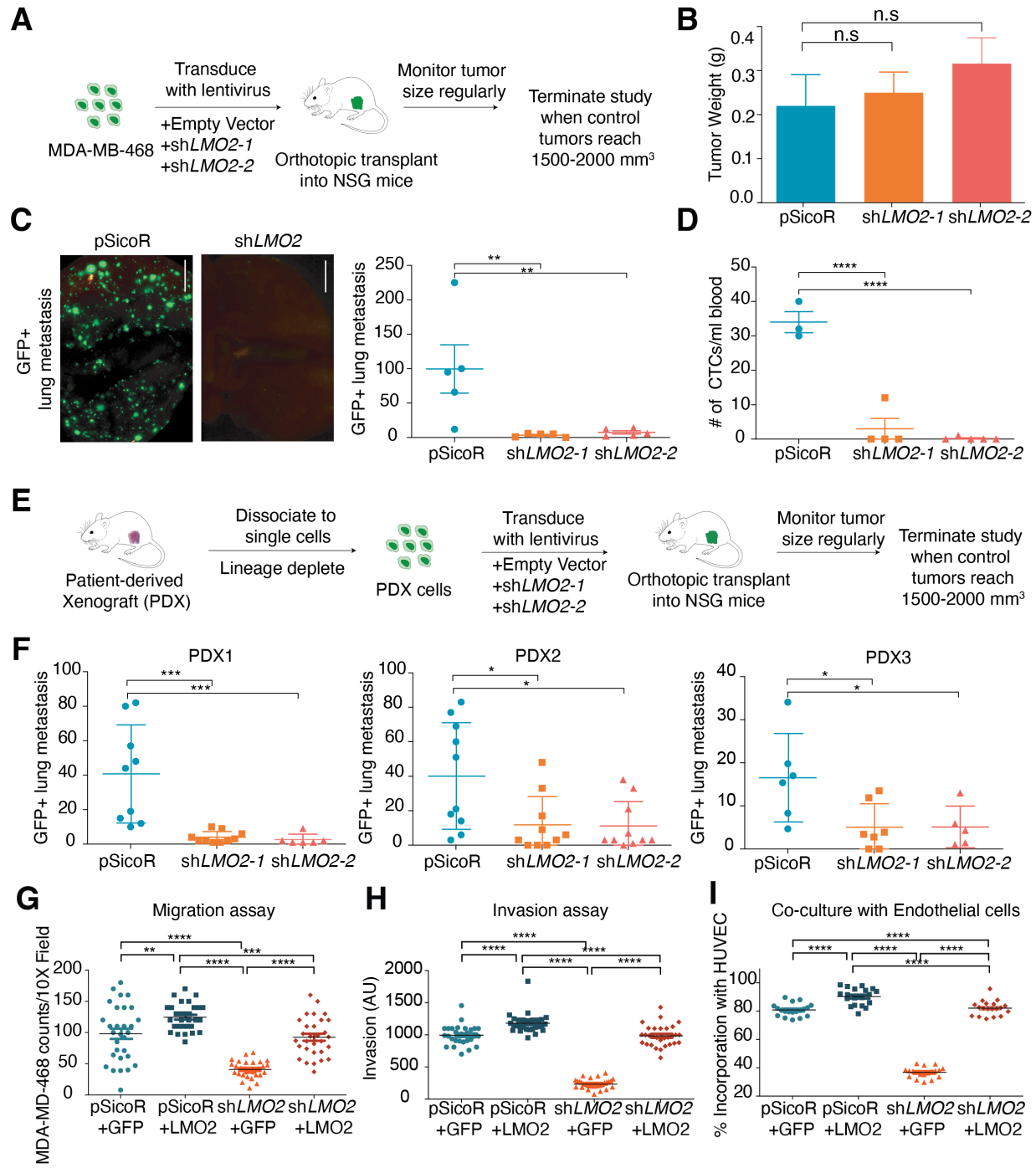
589 (D) Quantification of GFP<sup>+</sup> cells from *Lmo2-PyMT* tumors (*n*=5 mice).

590 (E) Representative immunofluorescence image of *Lmo2* lineage-traced cells (GFP<sup>+</sup>  
591 green) co-localizing and integrating with endomucin (magenta) stained tumor  
592 vasculature. High resolution magnification of Inset 1 and 2 are presented, Scale bar =  
593 50 $\mu$ m.

594 (F) Schematic diagram showing the experimental scheme for *Lmo2-PyMT* tumors  
595 treated with tamoxifen to trace metastatic cells.

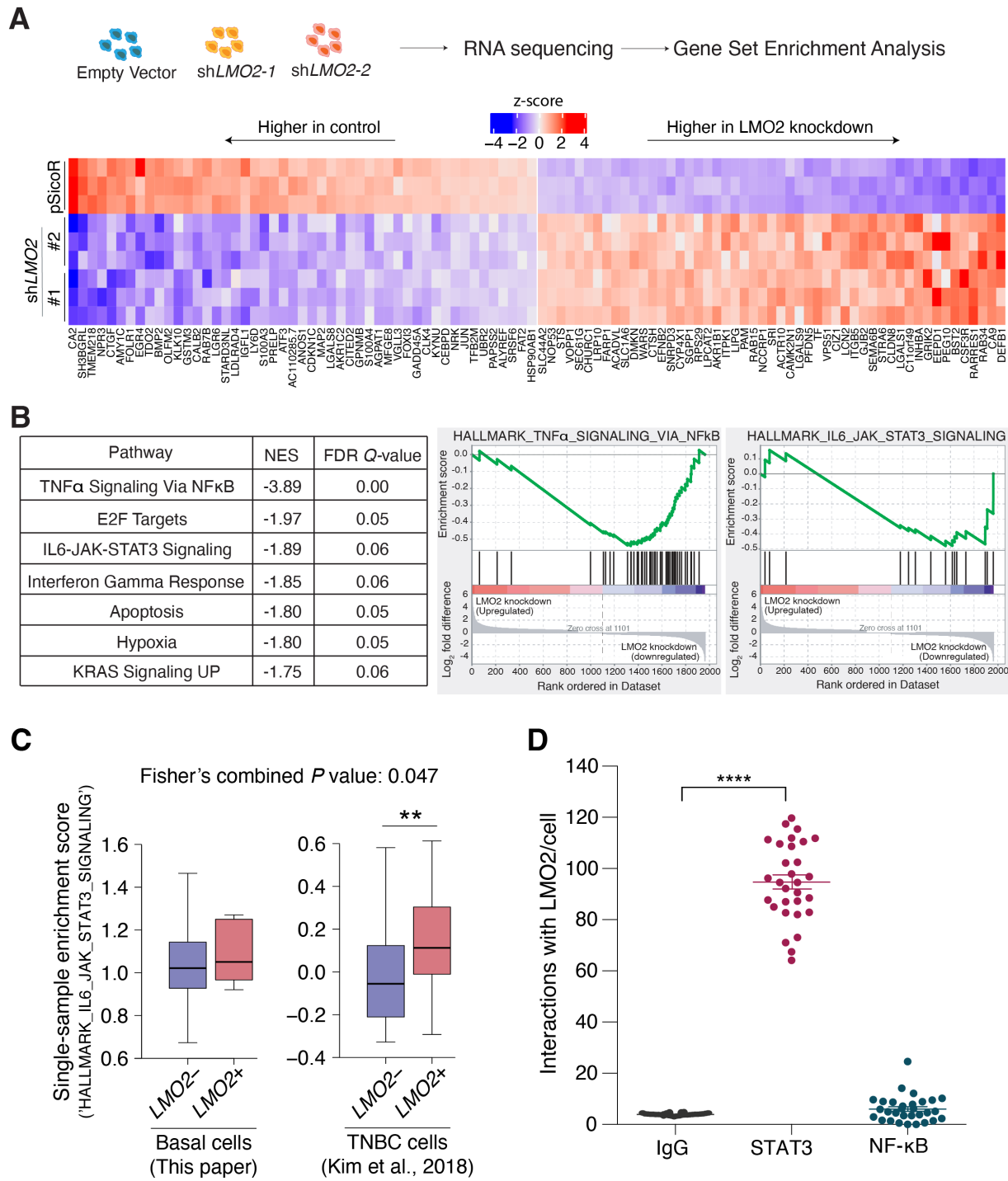
596 (G) *Panel 1*: FACS analysis of *Lmo2-PyMT* tumors at tumor end point from (F). Cells  
597 are gated on lineage<sup>-</sup> (CD45<sup>-</sup>, CD31<sup>-</sup>, Ter119<sup>-</sup>), DAPI<sup>-</sup> cells (See **Fig. S2**) and analyzed  
598 using TdTomato<sup>+</sup> and GFP<sup>+</sup>. *Panels 2 and 3*: EpCAM and CD49f expression status in  
599 GFP<sup>+</sup> and TdTomato<sup>+</sup> cells. *Panels 4*: Quantification of TdTomato<sup>+</sup> and GFP<sup>+</sup> cells from  
600 *Lmo2-PyMT* tumors (*n*=4 mice).

601 (H) *Panel 1*: Representative image of metastasis shown, Scale bar = 100 $\mu$ m. *Panel 2*:  
602 Quantification of total number and area of GFP<sup>+</sup> and TdTomato<sup>+</sup> lung metastasis in  
603 *Lmo2-PyMT* tumors. (n=4 mice) Data are shown as mean  $\pm$  SD, and statistical analysis  
604 was performed by unpaired, two-sided Wilcoxon rank sum test \*  $P<0.05$ .



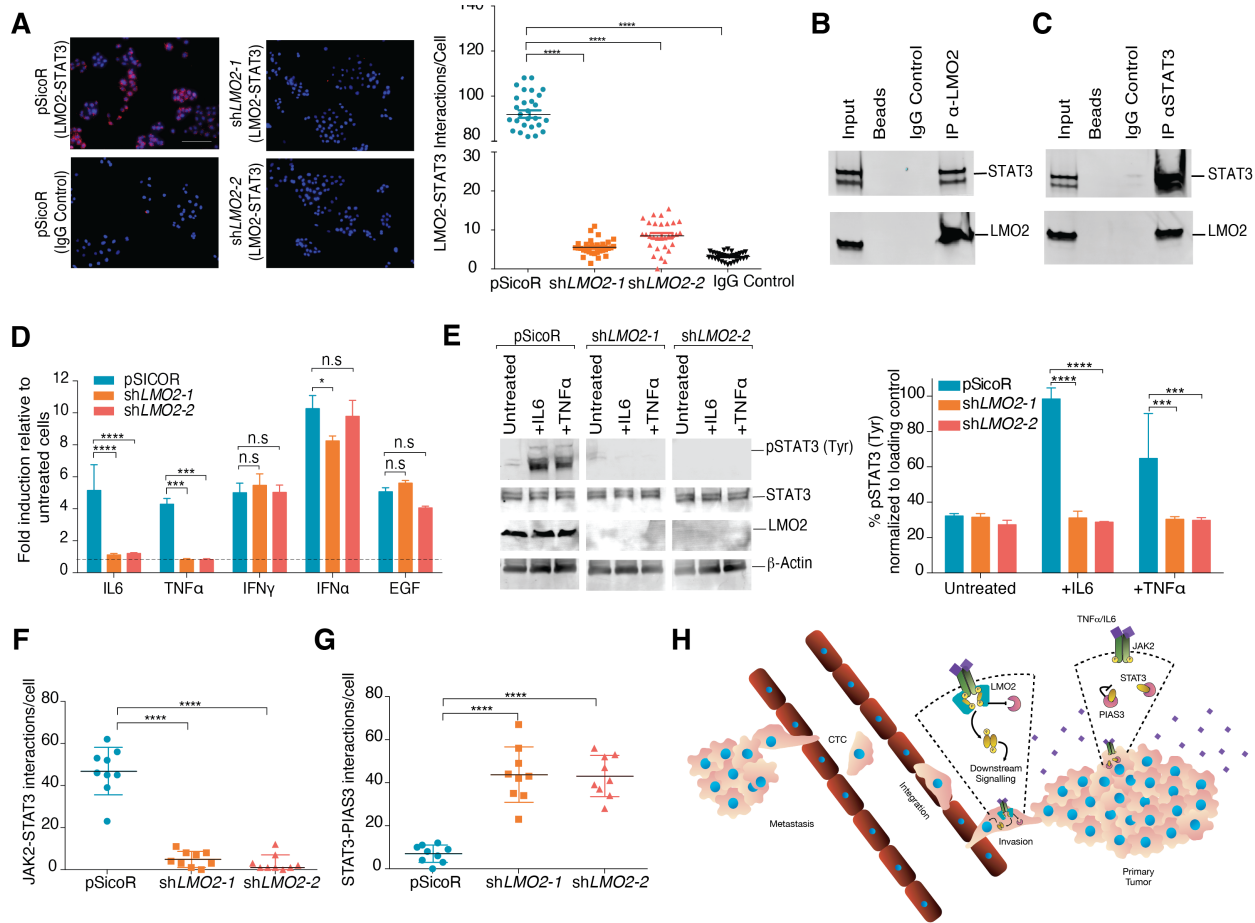
605 **Figure 3. Knockdown of LMO2 reduces lung metastasis in human breast cancer.**  
606 (A) Schematic of LMO2 knockdown in MDA-MB-468 cells followed by orthotopic  
607 transplant in NSG mice to evaluate tumor burden and metastases.  
608 (B) LMO2 knockdown in MDA-MB-468 cells. Tumor weight is shown with no significant  
609 difference between the control and LMO2 knockdown ( $n=5$  mice/group). Data are  
610 shown as mean  $\pm$  SD, and statistical analysis was performed by ANOVA with Dunnett's  
611 adjustment, n.s.  $P>0.05$

612 (C) LMO2 knockdown decreases the number of spontaneous GFP<sup>+</sup> lung metastasis in  
613 MDA-MB-468 cells ( $n=5$  mice/group). *Left panel*: representative immunofluorescence  
614 image with scale bar = 5mm, *right panel*: quantification. Data are shown as mean  $\pm$  SD,  
615 and statistical analysis was performed by ANOVA with Dunnett's adjustment, \*\*  
616  $P<0.01$ .  
617 (D) LMO2 knockdown decreases the number of circulating tumor cells in MDA-MB-468  
618 cells ( $n=3$  mice in pSicoR, 4 in shLMO2-1, 5 in shLMO2-2). Data are shown as mean  $\pm$   
619 SD, and statistical analysis was performed by ANOVA with Dunnett's adjustment, \*\*\*\*  
620  $P<0.0001$ .  
621 (E) Schematic of LMO2 knockdown in patient derived xenografts (PDXs) followed by  
622 orthotopic transplant in NSG mice to evaluate tumor burden and metastases.  
623 (F) LMO2 knockdown decreased number of spontaneous GFP<sup>+</sup> lung metastasis in PDX  
624 samples. Data are combined from 3 independent experiments for PDX1, PDX3 and  
625 from 2 independent experiment for PDX2 ( $n=9$  mice/ group for PDX1,  $n=6$  mice/group  
626 for PDX2,  $n=10$  mice/group for PDX3). Data are shown as mean  $\pm$  SD, and statistical  
627 analysis was performed by ANOVA with Dunnett's adjustment, \*  $P<0.05$ , \*\*  $P<0.01$ , \*\*\*  
628  $P<0.001$ , \*\*\*\*  $P<0.0001$ .  
629 (G) MDA-MB-468 cells infected with shRNA targeting 3' UTR of LMO2 or a control  
630 shRNA pSicoR were infected with either an empty vector control 'GFP' or an LMO2-  
631 overexpression vector '+LMO2' to generate pSicoR +GFP, pSicoR +LMO2, shLMO2  
632 +GFP, shLMO2 +LMO2. Transwell migration was quantification at 24 hours.  
633 (H) Spheroid invasion assay was performed and quantified at Day 5 using the breast  
634 cancer cells from (G).  
635 (I) The breast cancer cells from (G) were co-cultured with HUVEC cells and the  
636 percentage of breast cancer cells that are co-localizing with HUVEC tubes was  
637 quantified using ImageJ.  
638 For all experiments in (G-I),  $n=3$  and 10 images were analyzed per condition per  $n$ .  
639 Statistical analysis was performed by ANOVA with Dunnett's adjustment, and  
640 significance is indicated as \*\*  $P<0.01$ , \*\*\*  $P<0.001$ , \*\*\*\*  $P<0.0001$



641 **Figure 4: LMO2 regulates the IL6-JAK-STAT3 pathway and binds to STAT3**  
642 **(A)** Top: Schematic of bulk RNA-seq analysis in MDA-MB-468 cells infected  
643 with shRNAs targeting LMO2 or a control pSicoR. Bottom: Heatmap showing top and  
644 bottom 50 genes differentially expressed between control and LMO2 knockdown  
645 conditions, ordered by P-adjusted value.

646 (B) *Left*: Hallmark gene sets found to be significantly enriched by GSEA analysis.  
647 Normalized enrichment scores (corresponding to control pSicoR vs LMO2 knockdown)  
648 and FDR Q-values are determined by the GSEA software. An FDR Q-value cutoff of  
649 <0.25 was used to select significant gene sets. *Right*: Enrichment plots for  
650 'HALLMARK\_TNF $\alpha$ \_SIGNALING\_VIA  
651 \_NFkB' and 'HALLMARK\_IL6\_JAK\_STAT3\_SIGNALING' are depicted.  
652 (C) Differential enrichment of the 'HALLMARK\_IL6\_JAK\_STAT3\_SIGNALING' pathway  
653 in *LMO2*<sup>+</sup> vs. - cells from two independent human breast cancer datasets as described  
654 in **Fig. 1C**.  
655 (D) Proximity mediated ligation assay showed that LMO2 had a stronger interaction with  
656 STAT3 compared to NF-kB *in vitro* ( $n=3$ , 10 images were analyzed per condition per  $n$ ).  
657 Statistical analysis was performed by ANOVA with Dunnett's adjustment. \*\*\*\*  $P<0.0001$



658 **Figure 5: LMO2 stabilizes STAT3 signaling in breast cancer cells**

659 **(A)** Left panel: Proximity mediated ligation assay shows that LMO2 binds to STAT3 *in*  
660 *vitro* and this interaction is significantly reduced with LMO2 knockdown indicating  
661 specificity of the assay. Right panel: Quantification of  $n=3$  experiments and 10 images  
662 were analyzed per condition per  $n$ . Scale bar = 60 $\mu$ m. Statistical analysis was  
663 performed by ANOVA with Dunnett's adjustment, \*\*\*\*  $P<0.0001$ .

664 **(B)** Western blot of the input, immunoprecipitated beads (control), IgG (control) and  
665 LMO2 shows that LMO2 is able to pull-down STAT3. One representative blot of three  
666 independent experiments is shown.

667 **(C)** Western blot of the input, immunoprecipitated beads (control), IgG (control) and  
668 STAT3 shows that STAT3 is able to pull-down LMO2. One representative blot of three  
669 independent experiments is shown.

670 **(D)** STAT3-luciferase reporter activity shows robust stimulation of luciferase in control  
671 but not in cells with LMO2 knockdown when treated with IL6 and TNF $\alpha$ . IFN $\alpha$ , IFN $\gamma$ ,  
672 EGF treatment of cells results in robust stimulation in control and knockdown cells  
673 suggesting that LMO2 function is specific to IL6 and TNF $\alpha$ . Quantification of  $n=3$   
674 experiments. Statistical analysis was performed by 2-way ANOVA with Sidak's  
675 correction, and significance is indicated as \*\*  $P<0.01$ , \*\*\*  $P<0.001$ , n.s.  $P>0.05$ .

676 **(E)** Immunoblotting (left panel) and quantification (right panel) showed decreased  
677 phosphorylation of STAT3 at Tyr705 in LMO2 knockdown cells when treated with IL6

678 and TNF $\alpha$  indicating that LMO2 knockdown disrupts phosphorylation of STAT3.  
679 Quantification of  $n=3$  experiments. Statistical analysis was performed by 2-way ANOVA  
680 with Sidak's correction, and significance is indicated as \*\*\* $P<0.001$ , \*\*\*\*  $P<0.0001$ .  
681 (F) Interactions between STAT3 and JAK2 detected by proximity mediated ligation  
682 assay is reduced upon LMO2 knockdown indicating that LMO2 facilitates binding of  
683 STAT3 and JAK2. Quantification of  $n=3$  experiments. Statistical analysis was performed  
684 by ANOVA with Dunnett's adjustment, and significance is indicated as \*\*\*\*  $P<0.0001$ .  
685 (G) Interactions between STAT3 and PIAS3 detected by Proximity mediated ligation  
686 assay is increased upon LMO2 knockdown indicating that LMO2 prevents binding of  
687 STAT3 and PIAS3. Quantification of  $n=3$  experiments. Statistical analysis was  
688 performed by ANOVA with Dunnett's adjustment, and significance is indicated as \*\*\*\*  
689  $P<0.0001$ .  
690 (H) Schematic of proposed mechanism of LMO2 in breast cancer metastasis. Tumor  
691 cells that express LMO2 have stabilized STAT3 signaling in response to IL6 and TNF $\alpha$   
692 from the microenvironment, allowing these cells to intravasate into the circulation by  
693 incorporating into the vasculature.